Determination of land surface heat fluxes at different temporal scales overthe Tibetan Plateau

MA Yaoming [1, 2, 3], LEI Zhong[4, 5, 6], MA Weiqiang[1, 2]

1. *Key Laboratory of Tibetan Environment Changes and Land Surface Processes, Institute of Tibetan Plateau Research, the Chinese Academy of Sciences, Beijing* 100101*, China*;
2. *CAS Center for Excellence in Tibetan Plateau Earth Sciences, Beijing* 100101*, China*;
3. *University of Chinese Academy of Sciences, Beijing* 100049*, China*;
4. *School of Earth and Space Sciences, University of Science and Technology of China, Hefei* 230026*, China*;
5. *CAS Center for Excellence in Comparative Planetology, Hefei* 230026*, China*;
6. *Jiangsu Collaborative Innovation Center for Climate Change, Nanjing* 210023*, China*

Abstract: Surface energy budget components (such as net radiation flux, sensible heat flux, latent heat flux and soil heat flux) at multiple temporal scales have significant meaning for understanding the energy and water cycle over the Tibetan Plateau (TP). In the framework of ESA-MOST Dragon Programme 4, the Surface Energy Balance System (SEBS) was tested and used to derive surface heat fluxes at different temporal scales over the TP by a combination use of geostationary satellite (FY-2C) data, polar orbiting satellite (SPOT/VGT, Terra/MODIS) data and ITPCAS forcing data. The validation results show there is a good agreement between derived heat fluxes and in situ measurements from Third Pole Environment Observation and Research Platform (TPEORP), which means the feasibility to derive surface heat fluxes over heterogeneous landscapes by a combination use of geostationary and polar orbiting satellite data in SEBS. The RMSEs for net radiation flux, sensible heat flux, latent heat flux and soil heat flux are 76.63 Wm^{-2}, 60.29 Wm^{-2}, 64.65 Wm^{-2} and 37.5 Wm^{-2}, respectively. The diurnal, seasonal and inter-annual variation characteristics were also clearly identified through analyses of derived turbulent fluxes.

Key words: sensible heat flux, latent heat flux, parameterization, SEBS, the Tibetan Plateau

Citation format: Ma Y M,Lei Z and Ma W Q. 2020. Determination of land surface heat fluxes at different temporal scales overthe Tibetan Plateau. Journal of Remote Sensing(Chinese). 24(S1): 50−57

1 INTRODUCTION

The Third Pole Environment (TPE) centered on the Tibetan plateau and the Himalayas feeds Asia s largest rivers which provide water to 1.5 billion people across ten countries. Due to its high elevation, TPE plays a significant role in global atmospheric circulation and is highly sensitive to climate change. Intensive exchanges of water and energy fluxes take place between the Asian monsoon, the plateau land surface (lakes, glaciers, snow and permafrost) and the plateau atmosphere at various temporal and spatial scales. The TP is drawing increased attention among scientific community. How to derive land surface heat fluxes over the heterogeneous landscapes at different spatial and temporal scale becomes an important scientific problem.

At least three methods, in situ measurements, satellite remote sensing and numerical modeling, can be used to achieve land surface heat fluxes over the TP. The most accurate method is from field observation. A Third Pole Environment (TPE, Yao, et al. 2012) Observation and Research Platform (TPEORP), which including 21 stations scattered through the TP have been set up (Ma, et al. 2008). The surface heat flux at different land surface type can be achieved. However, because of severe natural environment and complex landscape of the TP, the observation stations are not only sparse but also uneven there. For the time being, there are few stations in the vast area of northwestern part of the TP. Furthermore, the greatest shortage of field observation is its limit spatial representativeness. It's impossible to derive plateau scale land surface heat flux only through in situ measurements.

The second choice is to operate an atmospheric model. Numerical simulation models of regional heat fluxes have been developed for a range of scales and with different levels of physical complexity in the TP (Sen, et al. 2004; Xue, et al. 2004; Sato, et al. 2005; Yang, et al. 2007; Meng, et al. 2009). Because the interactions between soil, vegetation and atmosphere vary both spatially and temporally, regional heat fluxes in heterogeneous natural landscapes are difficult to predict accurately by means of atmospheric models

Received: 2019-10-21; **Accepted:** 2020-04-16

Foundation: CLIMATE-TPE (ID 32070) in the framework of the ESA-MOST Dragon 4 Programme; the National Natural Science Foundation of China (No. 91837208, 41661144043, 41875031, 41522501, 41830650); Strategic Priority Research Program of Chinese Academy of Sciences (No. XDA20060101); the Chinese Academy of Sciences (No. QYZDJ-SSW-DQC019)

First author biography: MA Yaoming (1964—), male, professor. His research interest mainly focus on atmospheric boundary layer physics and application of remote sensing. E-mail: ymma@itpcas.ac.cn

Corresponding author biography: Lei Zhong (1979—), male, professor. His main research interests focus on land-atmosphere interaction and application of remote sensing. E-mail: zhonglei@ustc.edu.cn

only. Most atmospheric models deal with terrestrial landscapes by assuming homogeneity of system variables and processes within each model grid. The coarse model spatial resolution also limits to looking into some sub-grid information.

Fortunately, satellite remote sensing technology can partially make up for above deficiencies. The remote sensing approaches are utilized to describe land surface characteristic parameters on a regional or even global scale (Tucker, 1987; Wan and Dozier, 1989; Becker and Li, 1990; Sellers, et al. 1990; Price, 1992). These parameters include surface temperature, surface albedo, Normalized Difference Vegetation Index (NDVI), Modified Soil Adjusted Vegetation Index (MSAVI), vegetation fractional cover, Leaf Area Index (LAI) and surface thermal emissivity (Susskind, et al. 1984; Tucker, 1987; Wan and Dozier, 1989; Becker and Li, 1990; Sellers, et al. 1990; Price, 1992; Price, 1993; Li and Becker, 1993; Qi, et al. 1994; Price, 1994; Kustas and Norman, 1997; Carlson and Ripley, 1997; Ma, et al. 2002; Ma, et al. 2003; Liang, 2004;). Regional heat fluxes can be determined indirectly with the aid of these land surface variables (Ma, et al. 2014). Recent studies have explored several approaches to estimate the regional distribution of surface heat fluxes in the Tibetan Plateau and adjacent arid and semi-arid region of northwest of China (Wang, et al. 1995; Ma, et al. 2002; Ma, et al. 2003; Jia, 2004; Ma, et al. 2006). These methods bridge the gap between the point/local measurements and the regional scale. Most studies of the regional distribution of land surface heat fluxes have been performed in meso scale regions by using polar orbiting satellite data. Investigations in heterogeneous landscapes of whole Tibetan Plateau were rare. Furthermore, little information about the diurnal, seasonal and interannual variations have been got, which hampers the understanding of land atmosphere interactions in the TP at multi-temporal scale.

Based on polar-orbiting and geostationary satellite data, this paper aims to develop a better satellite remote sensing parameterization methodology of regional land surface heat fluxes over heterogeneous landscapes of whole Tibetan Plateau by including surface layer and atmospheric boundary layer observations. The land surface heat flux changing trends at different temporal scales will be identified. The structure of the article is as below. The introduction of the data and methodology adopted in this study is introduced in Section 2. The validation results of surface heat flux and its changing characteristics are presented in Section 3. The last part provides the main conclusions and future work plan.

2 DATA AND METHODOLOGY

2.1 Data

The data used in this paper mainly include datellite data (FY-2C/SVISSR, SPOT/VGT, Terra/MODIS). The in-situ observation data from TPEORP were used to validate model results. Taking data completeness and continuity into account, six stations equipped with flux measurements were selected, namely, BJ, D105, MS3478, Nam Co, Linzhi and QOMS (Qomolangma Station for Atmospheric Environmental Observation and Research, Chinese Academy of Sciences (CAS)) (Fig. 1).

Both geostationary satellite (FY-2C/SVISSR) and polar orbiting satellite (SPOT/VGT, Terra/MODIS) will be used to derive the essential land surface paramters, such as surface temperature (T_s), surface albedo(α), surface emissivity(ε_s), Normalized Difference Vegetation Index (NDVI), vegetation fractional cover (P_v) (Tucker, 1987 ; Becker and Li, 1990 ; Carlson and Ripley, 1997 ; Ma, et al. 2002, 2003 ; Zhong, et al. 2010, 2012). The FY-2C, as the fourth satellite of the FY series and the first meteorological satellite operated by China, became completely operational in 2006. SVISSR is the major sensor onboard the FY-2C, consisting of four infrared channels (FIR1: 10.3—11.3 μm, FIR2: 11.5—12.5μm, FIR3: 6.3—7.6 μm, MIR: 3.5—4.0 μm) and one visible channel (VIS: 0.55—0.90 μm) (Ouyang and Li, 2012). The hourly T_s will be retrieved by a split window algorithm (Hu, et al. 2018). Other paramters (α, ε_s, NDVI, P_v), which supposed have little diuanal variation, will be retrieved from SPOT/VGT.

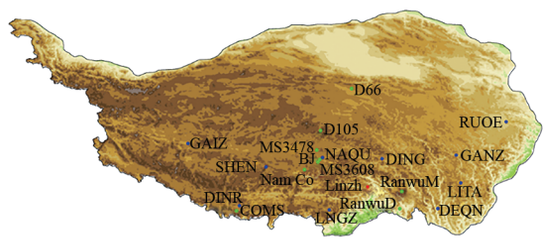

Fig. 1 The location of meteorological stations in the Tibetan Plateau

The meteorological forcing data, such as downward shortwave radiation, downward longwave radiation, air temperature, specific humidity, wind speed, is from Institute of Tibetan Plateau Research. This data set has the highest spatiotemporal resolution of any of the reanalysis data. The data set merges observations from 740 operatiaonal weather stations operated by China Meterological Administration.

2.2 Methodology

A Surface Energy Balance System (SEBS) proposed by Su (2002) was used in this study to derive the energy balance components, such as the net radiation flux (R_n), sensible heat flux (H), latent heat flux (LE) and soil heat flux (G_0). The SEBS model was an extending of Surface Energy Balance Index(SEBI) concept with adynamic model for thermal roughness (Su, et al., 2001) and the Bulk Atmospheric Similarity (BAS) theory of Brutsaert (1999) for PBL scaling and the Monin-Obukhov Atmospheric Surface Layer (ASL) similarity for surface layer scaling such that SEBS can be used for both local scaling and regional scaling under all atmospheric stability regimes thus providing a link for radiometric measurements and atmospheric models at various scales. The general procedure for estimation of surface heat flux is shown in Fig. 2. The detailed equations to derive $R_n, H, LE,$ *and* G_0 were shown as followings.

2.2.1 Net radiation flux

The regional net radiation flux R_n can be derived from

$$\begin{aligned} R_n &= S\downarrow - S\uparrow + L\downarrow - L\uparrow \\ &= (1-\alpha)S\downarrow + L\downarrow - \varepsilon_s \sigma T_s \end{aligned} \quad (1)$$

where S and L represent the downwelling short-wave and long wave radiation, resectively. Surface albedo can be derived from integrated hemispherical planetary reflectance (Liang, et al. 2001 ; Ma, et al. 2003 ; Zhong, et al. 2012). Surface emissivity (ε_s) was estimated by a semi-emipirical relationship with vegetation index (Zhong et al. 2010). The surface temperature can be retrieved by split window algorithm based on two thermal infrared channels onboard FY-2C/SVISSR (Hu et al. 2018).

2.2.2 Sensible heat flux

The sensible heat flux (H) can be calculated by the Monin-Obukhov (M-O) similarity theory

$$u_* = ku\left(\ln\left(\frac{z-d_0}{z_{0m}}\right) - \Psi_m\left(\frac{z-d_0}{L}\right) + \Psi_m\left(\frac{z_{0m}}{L}\right)\right)^{-1}$$

(2)

$$H = ku_*\rho C_p(\theta_0 - \theta_a)\left(\ln\left(\frac{z-d_0}{z_{0h}}\right) - \Psi_h\left(\frac{z-d_0}{L}\right) + \Psi_h\left(\frac{z_{0h}}{L}\right)\right)^{-1} \quad (3)$$

where k = 0.4 is the von Karman's constant; u (m/s) is the mean wind speed; d_0 (m) is the zero plane displacement height; z_{0m} (m) is the roughness height of momentum transfer; u_* (m/s) is the friction velocity; ρ (kg/m^3) is the density of air; C_p (J/(kg·K)) is the specific heat for moist air; z_{0h} (m) is the scalar roughness height of heat transfer; and θ_0 (K) and θ_a (K) are the potential temperature at the surface and the potential air temperature at the reference height respectively. Ψ_m and Ψ_h are the stability correction functions for the momentum and sensible heat transfers and L is the M-O length.

2.2.3 Soil heat flux

The soil heat flux (G_0) is determined by net radiation flux and vegetation coverage.

$$G_0 = R_n[\Gamma_v + (1 - P_v)(\Gamma_s - \Gamma_v)] \quad (4)$$

where Γ_v and Γ_c are ratios of soil heat flux and net radiation flux for bare soil and full vegetation cover. P_v is vegetation coverage.

2.2.4 Latent heat flux

The latent heat flux (*LE*) can be derived from relative evaporative fraction and latent heat flux under wet-limit condition as

$$\mathrm{LE} = \Lambda_r LE_{wet} \quad (5)$$

where Λ_r is relative evaporative fraction. It can be derived from actual sensible heat flux (H) and sensible heat flux at the wet limit (H_{wet}) and dry limit (H_{dry}) as

$$\Lambda_r = 1 - \frac{H - H_{wet}}{H_{dry} - H_{wet}} \quad (6)$$

where H_{wet} and H_{dry} can be calculated from the energy balance equation at wet limit and dry limit, respectively.

3 RESLUTS AND DISCUSSION

The Root Mean Square Error (RMSE), Mean Bias (MB), Mean Absolute Error (MAE) and R (Correlation Coefficient) were used to make a comparison between derived surface heat fluxes and in situ measurements from 6 flux towers. As shown in Table 1, there is a good agreement between satellite estimation and field measurements, with average RMSE for $R_n, H, LE, and\ G_0$ of about 76.63 Wm^{-2}, 60.29 Wm^{-2}, 64.65 Wm^{-2} and 37.5 Wm^{-2}, respectively. The total validation numbers (N) are more than 3800 to make the results much more robust and convincible. It means the surface energy balance system for determination of regional distribution of land surface heat fluxes is reasonable and it can be used over the TP area.

Table 1 Comparsions of the derived net radiation flux, sensible heat flux, latent heat flux and soil heat flux versus the measured values at six flux tower stations in the Tibetan Plateau

Indicators	*Rn*	*H*	*LE*	G_0
RMSE	76.63	60.29	64.65	37.5
MB	−3.11	−22.13	6.03	7.81
MAE	50.47	45.67	44.39	28.43
R	0.935	0.789	0.792	0.791
N	4720	4554	3865	3837

Based on the hourly information of turbulent heat fluxes, the seasonal evolution with the Asian monsoon and their spatial distribution maps have been generated. As shown in Fig.4(a), the spatial distribution of sensible heat flux is a little complex because the sensible heat flux is determined by multiple factors such as surface temperature, air temperature, wind speed, land-atmosphere heat exchange coefficient, etc. There is a clear spatial distribution characteristic for latent heat flux especially in summer (Fig. 4(b)). The southeastern part of the TP usually has much higher latent heat flux than northwestern part. This spatial distribution is in accordance with the climate conditions and vegetation distributions of the TP. It's well-known that the southeast of TP usually tends to be much warmer and humid than northwest part. Because the TP is under the influence of the Asian summer monsoon, the seasonal variation of turbulent heat flux can be also clearly identified. From pre-monsoon to monsoon season (Jan. to May), the sensible heat flux usually increased to its maximum while the latent heat flux increased a little bit because of the rising solar elevation. In the monsoon season (Jun. to Sep.), with a lot of evapotranspiration taking place especially in the southeast part of the TP, the latent heat flux increased to its maximum while the sensible heat flux decreased. In the post-monsoon season (Oct. to Dec.), both the sensible heat flux and latent heat flux tend to decrease because of the descending solar elevation.

The diurnal, seasonal and inter-annual variations and regional distributions of net radiation flux, sensible heat flux, latent heat flux and soil heat flux over the TP area were derived by using the parameterization scheme above. As shown in Fig.3a, a typical diurnal variation pattern of sensible heat flux and latent heat flux can be clearly identified. In the evening (from 19 h to 09 h, Beijing Standard Time, BST), when there is no input solar energy, the land surface heat flux tends to be very smooth with negative or a small positive value. After that, from 10 h to 15 h, with the increase of solar elevation, the sensible heat flux increases gradually to its maximum. Then it decreases again with the descending of solar elevation. After 19:00, the variation of sensible heat flux tends to be small and smooth again. An opposite trend can be found in variations of latent heat flux (Fig. 3(b)). What can also be found in Fig.3 is that the increasing process of sensible heat flux and latent heat flux is a little slowly (from 07 h to 15 h) than their decreasing process (from 15 h to 19 h). This diurnal variation has a close relationship with the diurnal variation of atmospheric boundary layer because major driving force for the atmospheric circulation is from the turbulent heat flux. Therefore, the information of plateau scale will have great importance for understanding the weather conditions in the Third Pole region and its surroundings.

Based on MODIS data and related meteorological forcing data, a long time series land surface heat flux dataset was retrieved. The annual variation trends of sensible heat flux and latent heat flux in the TP from 2001 to 2016 are shown in Fig. 5. Both increasing and decreasing of turbulent heat fluxes exist in the TP. In general, sensible heat flux showed a significant increase across the whole TP, especially in the central and southeast part of the TP whose increases are significant. However, it showed a decrease in the central-northern TP. Latent heat flux showed slightly decrease across most parts of the TP and it showed increases in the west and north edge of the TP, and eastern TP. The western and eastern TP play different role in driving atmospheric circulation. If the TP is divided according to 90°E, it can be easily found that the surface sensible heating increases while the latent heating decreases in the western TP from

2001 to 2016. For the west and north edge of the TP, the glacier melting under the warming climate conditions could lead to increasing of the latent heat flux and decreasing trend of sensible heat flux. For the eastern part of the TP, both increasing and decreasing of turbulent heat flux exist. The changing trends in different regions appear dramatically different due to different land surface types and climate conditions.

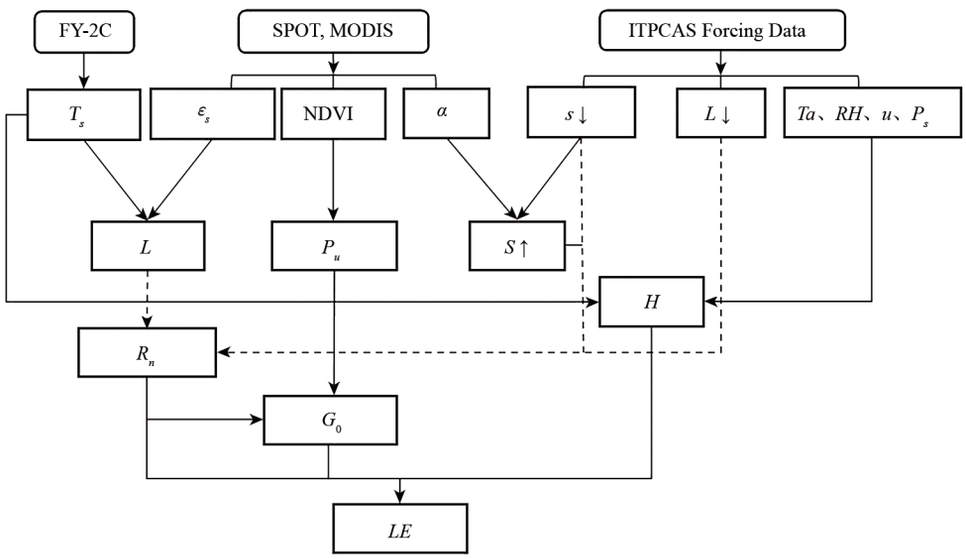

Fig. 2 Diagram of parameterization procedure by combing satellite data with in situ measurements

4 CONCLUDNG REMARKS

In this study, the regional distribution of plateau scale net radiation flux, sensible heat flux, latent heat flux and soil heat flux over heterogeneous landscape were determined by using the in situ data from TPEORP, satellite data, ITPCAS forcing data and SEBS model. The geostationary satellite (FY-2C/SVISSR) was used to derive the hourly land surface temperature, while other land surface variables (such as vegetation index, surface albedo, surface emissivity) were supposed have very little diurnal variation and were retrieved from polar orbiting satellites (SPOT/VGT, Terra/MODIS). Therefore, the derived turbulent heat fluxes have the temporal scale from hourly, monthly to annual. Compared with the in situ measurements at 6 stations in TPEORP, the RMSE for net radiation heat flux, sensible heat flux, latent heat flux and soil heat flux are 76.63 Wm^{-2}, 60.29 Wm^{-2}, 64.65 Wm^{-2} and 37.5 Wm^{-2}, respectively. The correlation coefficients for those four energy budget components are 0.935, 0.789, 0.792 and 0.791, respectively. The validation results proved the feasibility to derive large scale turbulent fluxes by a combination use of geostationary and polar orbiting satellite data. The analyses of derived turbulent fluxes show the following phenomenon.

(1) Typical diurnal variation of sensible heat flux and latent heat flux exist, which is corresponding to the diurnal variation of downwelling shortwave and longwave radiation. It's also in good agreement with daily atmospheric boundary layer changing characteristic.

(2) Under the influence of Asian Summer Monsoon, the seasonal variations of sensible heat flux and latent heat flux in the TP can be clearly identified. The sensible heat flux dominates in the pre-monsoon and post-monsoon season while the latent heat flux dominates in the monsoon season. The sensible heat flux in the monsoon season exhibits southeast high and northwest low pattern which is caused by climate and land surface conditions in the TP.

(3) Interannual analyses of 16 years of turbulent heat fluxes show that for the western part of the TP, the sensible heat flux tends to increase while the latent heat flux tends to decrease. For the west and north edge of the TP, the glacier melting under the warming climate conditions could lead to increasing of the latent heat flux and decreasing of sensible heat flux.

Through two years' efforts, several main achievements have been acquired to promote the understanding of water and energy cycles over the Tibetan Plateau in CLIMATE-TPE project of Dragon 4. However, determination of surface energy budget components over heterogeneous landscape is not an easy task. The method used in this study is still in developing stage. Some assumptions were still used in this study. More stations need to be set up especially for the vast area of the northwest part of the TP, where has been proved having largest land surface temperature variance. Furthermore, some new satellites, for example FY-4, is worthy to be used to overcome the shortage of relatively low spectral and spatial resolution of FY-2. These research works will be done in next two years within the framework of Dragon 4 programme.

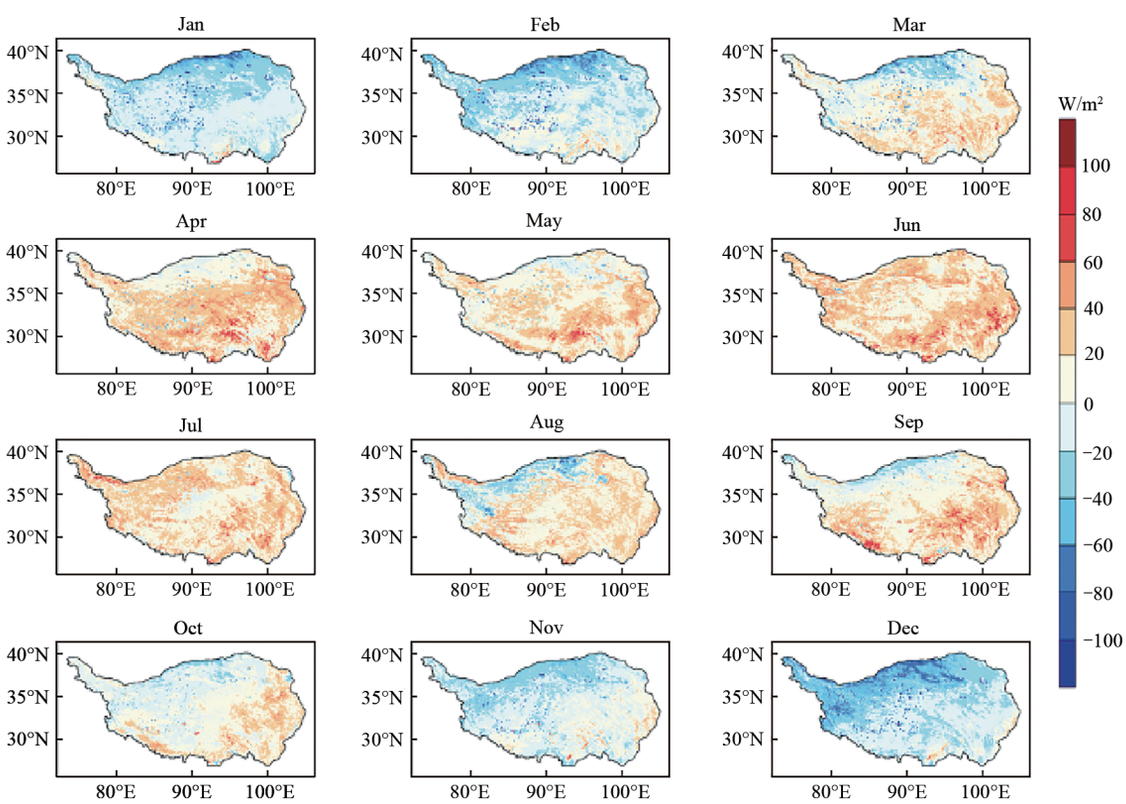

(a) Latent heat flux

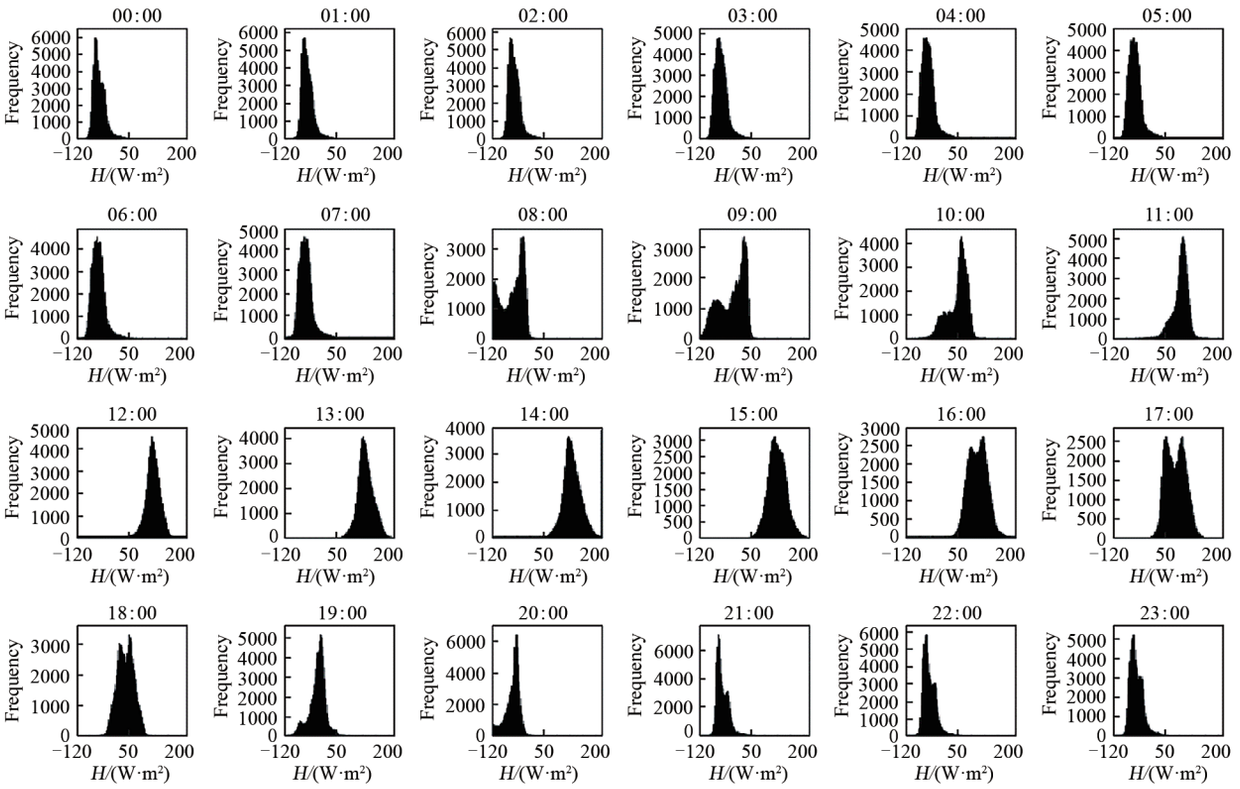

(a) Latent heat flux

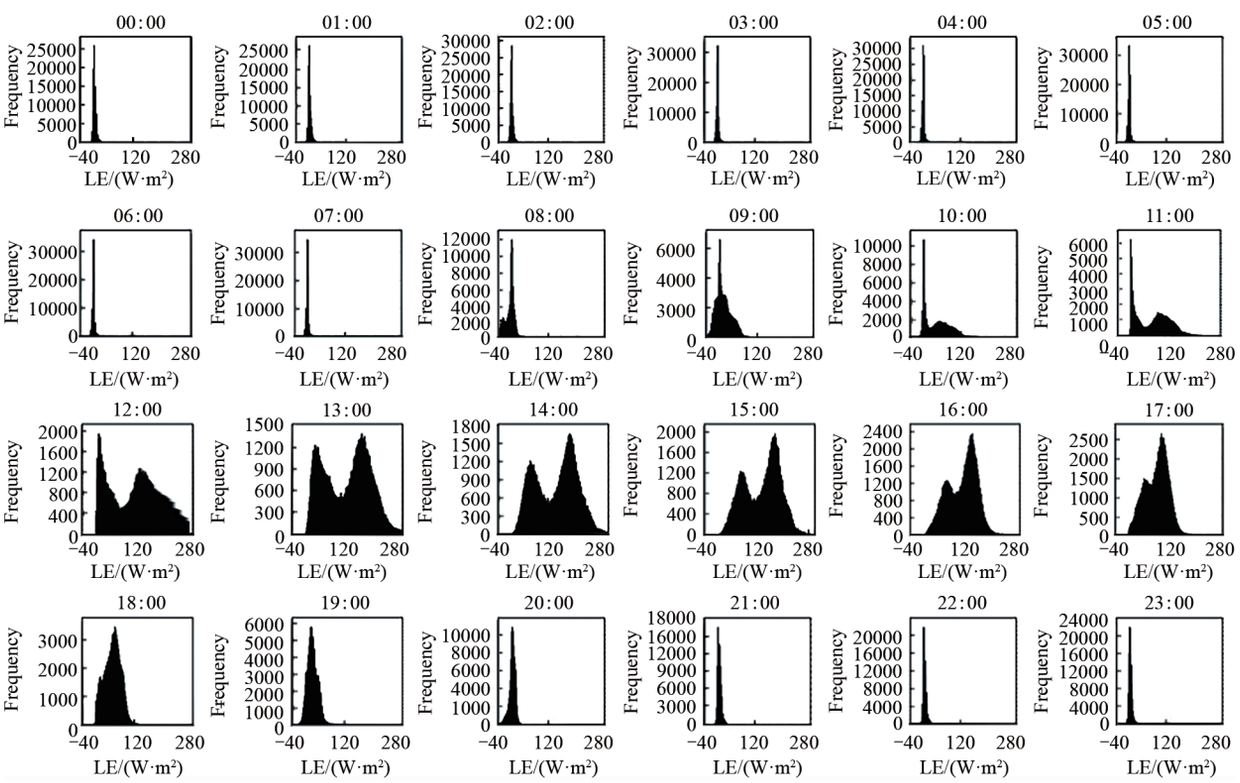

(b) Tibetan Plateau

Fig. 3 Frequency distribution histogram of yearly mean diurnal variations of sensible heat flux

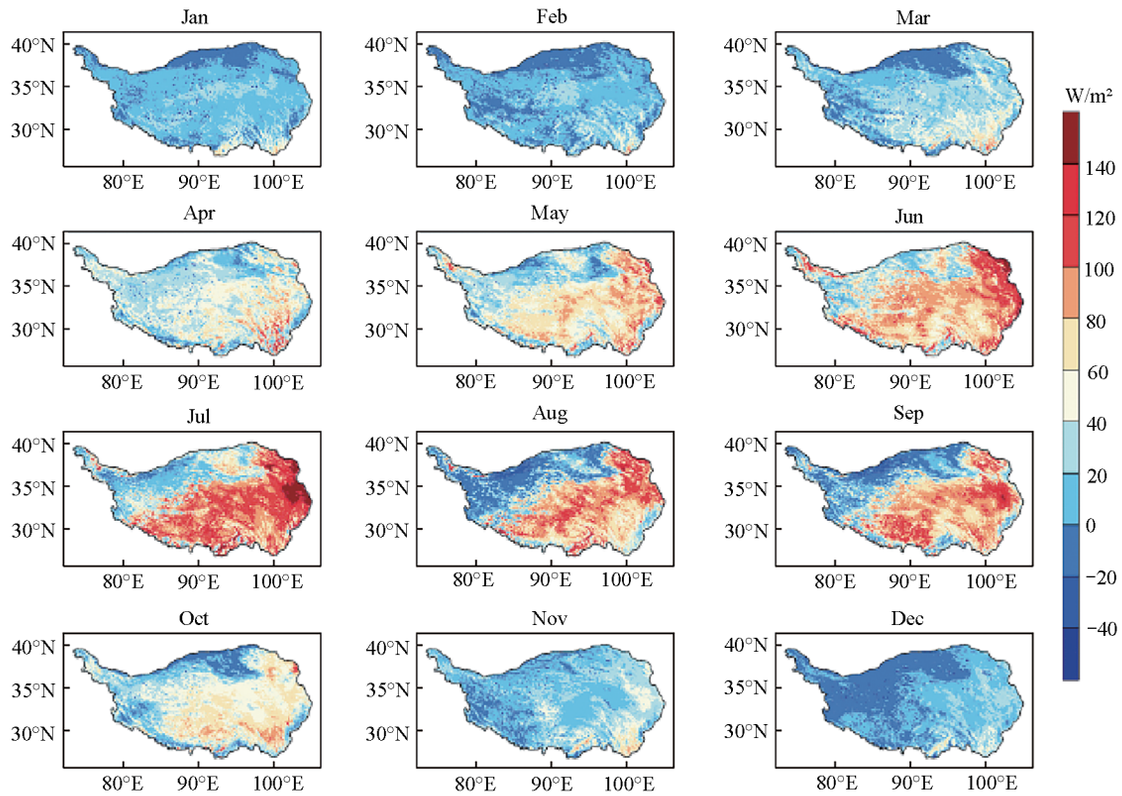

(b) Tibetan Plateau

Fig. 4 Seasonal variations of sensible heat flux

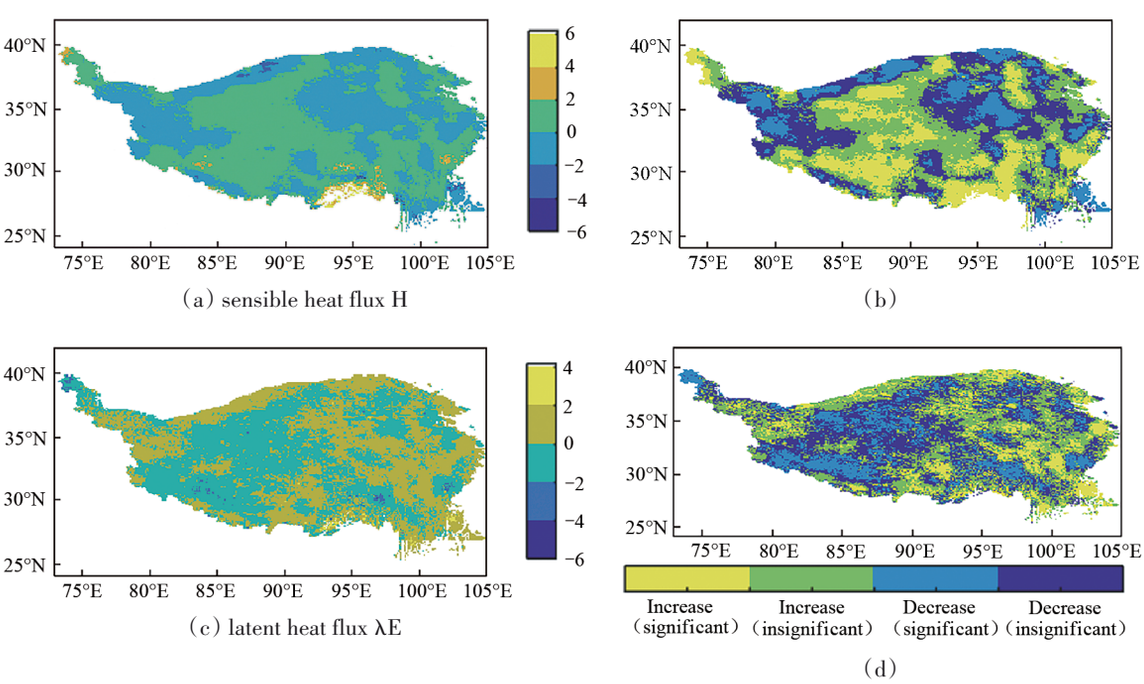

(a) sensible heat flux H (b)

(c) latent heat flux λE (d)

Fig. 5 Linear trends (left column) and significance test (right column) maps of (a) and (c) from 2001 to 2016. The trends were classified into four categories (b and d) according to statistical linear trend analysis: a significant increase ($p<0.05$), a significant decrease ($p<0.05$), an insignificant increase ($p>0.05$), and an insignificant decrease ($p>0.05$)

REFERENCES

Becker F and Li Z. 1990. Towards a local split window method over land surfaces. Remote Sensing, 11(3):369-393.

Brutsaert W. 1999. Aspects of bulk atmospheric boundary layer similarity under free-convective conditions. Reviews of Geophysics, 37 (4):439-451.

Carlson T N and Ripley D A. 1997. On the relation between NDVI, fractional vegetation cover, and leaf area index. Remote Sensing of Environment, 62(3):241-252.

Hu Y, Zhong L, Ma Y, Zou M, Xu K, Huang Z, and Feng L. 2018. Estimation of the land surface temperature over the Tibetan Plateau by using Chinese FY-2C geostationary satellite data. Sensors, 18, 376, DOI:10.3390/s18020376.

Jia L. 2004. Modeling heat exchanges at land-atmosphere interface using multi-angular thermal infrared measurements. Wageningen: Wageningen University, 199pp.

Kustas W P and Norman J M. 1997. A two-source approach for estimating turbulent fluxes using multiple angle thermal infrared observations. Water Resources Research, 33:1495-1508.

Liang S. 2000. Narrowband to broadband conversions of land surface albedo I Algorithms. Remote Sensing of Environment, 76(2): 213-238.

Liang S. 2004. Quantitative Remote Sensing of Land Surfaces. Hoboken: John Wiley and Sons, 534pp.

Li Z L and Becker F. 1993. Feasibility of land surface temperature and emissivity determination from AVHRR data. Remote Sensing of Environment, 43(1):67-85.

Ma Y, Kang S, Zhu L, Xu B, Tian T and Yao T. 2008. Tibetan observation and research platform-atmosphere-land interaction over a heterogeneous landscape. Bulletin of the American Meteorological Society, 89:1487–1492.

Ma Y, Su Z, Koike T, Yao T, Ishikawa H, Ueno K and Menenti M. 2003. On measuring and remote sensing surface energy partitioning over the Tibetan Plateau – – from GAME/Tibet to CAMP/Tibet. Physics and Chemistry of the Earth, 28(1):63-74.

Ma Y, Tsukamoto O, Ishikawa H, Su Z, Menenti M, Wang J and Wen J. 2002. Determination of regional land surface heat flux densities over heterogeneous landscape of HEIFE Integrating satellite remote sensing with field observations. Journal of the Meteorological Society of Japan, 80(3):485-501.

Ma Y, Zhong L, Su Z, Ishikawa H, Menenti M and Koike T. 2006. Determination of regional distributions and seasonal variations of land surface heat fluxes from Landsat-7 Enhanced Thematic Mapper data over the central Tibetan Plateau area. Journal of Geophysical Research Atmospheres, D10305, doi:10.1029/2005JD006742.

Ma Y, Zhu Z, Zhong L, Wang B, Han C, Wang Z, Lu L, Amatyal P M, Ma W and Hu Z. 2014. Combining MODIS, AVHRR and in situ data for evapotranspiration estimation over heterogeneous landscape of the Tibetan Plateau. Atmospheric Chemistry and Physics, 14:1507-1515.

Meng X, Lü S, Zhang T, Guo J, Gao Y, Bao Y, Wen L, Luo S and Liu Y. 2009. Numerical simulations of the atmospheric and land conditions over the Jinta oasis in northwestern China with satellite-derived land surface parameters. Journal of Geophysical Research Atmospheres, DOI: 10.1029/2008JD010360.

Oku Y and Ishikawa H. 2004. Estimation of land surface temperature over the Tibetan Plateau using GMS data. Journal Applied Meteorology, 43(4):548-561.

Ouyang X, Li J. 2012. Retrieval of land surface temperature by cross-calibrated SVISSR thermal infrared data onboard China geostationary satellite. Land Surface Remote Sensing, 85241X, doi: 10.1117/12.977598

Price J C. 1992. Estimating vegetation amount from visible and near infrared reflectances. Remote Sensing of Environment, 41(1):29-34.

Price J C. 1993. Estimating leaf area index from satellite data. IEEE Transactions on Geoscience and Remote Sensing, 31(3):727-734.

Qi J, Chehbouni A, Huete A R, Kerr Y H and Sorooshian S. 2015. A modified soil adjusted vegetation index. Remote Sensing of Environment, 48(2):119-126.

Sato T and Kimura F. 2005. Impact of diabatic heating over the Tibetan Plateau on subsidence over northeast Asian arid region. Geophysical Research Letters, DOI:10.1029/2004GL022089.

Sen O, Wang B and Wang Y. 2004. Impacts of re-greening the desertified lands in northwestern china: implications from a regional climate model experiment. Journal of the Meteorological Society of Japan, 82(6):1679-1693.

Sellers P J, Rasool S I and Bolle H J. 1990. A review of satellite data algorithms for studies of the land surface. Bulletin American Meteorological Society, 71(12):1429-1447.

Susskind J, Rosenfield J, Reuter D and Chahine M T. 1984. Remote sensing of weather and climate parameters from HIRS2/MSU on TIROS-N. Journal of Geophysical Research Atmospheres, 89 (D3):4677-4697.

Su Z. 2002. The Surface Energy Balance System (SEBS) for estimation of turbulent heat fluxes, Hydrology and Earth System Science, 6(1):85-99.

Su Z, Schmugge T, Kustas W P and Massman WJ. 2001. An evaluation of two models for estimation of the roughness height for heat transfer between the land surface and the atmosphere. American Meteorological Society, 40(11):1933-1951.

Tucker C J. 1987. Monitoring the grasslands of semi-arid Africa using NOAA AVHRR data. Remote Sensing, 7-11:1383-1622.

Wang J, Ma Y, Menenti M, Bastiaanssen W and Mistsuta Y. 1995. The scaling-up of processes in the heterogeneous landscape of HEIFE with the aid of satellite remote sensing. Journal of the Meteorological Society of Japan, 73(6):1235–1244.

Wan Z and Dozier J. 1989. Land surface temperature measurement from space: Physical principles and inverse modelling. IEEE Transactions on Geoscience and Remote Sensing, 27(3): 268-278.

Xue Y, Juang H M H, Li W P, Prince S, DeFries R, Jiao Y and Vasic R. 2004. Role of land surface processes in monsoon development: East Asia and West Africa. Journal of Geophysical Research Atmospheres, DOI:10.1029/2003JD003556.

Yang K, Watanabe T, Koike T, Li X, Fujii H, Tamagawa K, Ma Y and Ishikawa H. 2007. Auto-calibration system developed to assimilate AMSR-E data into a land surface model for estimating soil moisture and the surface energy budget. Journal of the Meteorological Society of Japan, 85A:229-242.

Yao T, Thompson L G, Mosbrugger V, Zhang F, Luo T, Xu B, Yang X, Joswiak D R, Wang W, Joswiak M E, Devkota L P, Tayal S, Jilani R and Fayziev R. 2012. Third pole environment (TPE). Environmental Development, 3(1):52-64.

Zhong L, Ma Y, Ma W, Fu Y, Su Z, Salama S, Chu D and Bianba C. 2012. Remote sensing of land surface parameters in the middle reaches of YarlungZangbo river and its two tributaries from AVHRR and MODIS data. Journal of the Meteorological Society of Japan, 90C:75-86.

Zhong L, Ma Y, Su Z and Salama M S. 2010. Estimation of land surface temperature over the Tibetan Plateau using AVHRR and MODIS data. Advances in Atmospheric Sciences, 27(5):1110-1118.